doi:10.1017/S1431927622002707
Microsc. Microanal. 28 (Suppl 1), 2022
© Microscopy Society of America 2022

Fully Quantitative Mapping of Igneous Phenocrysts By EPMA Using Mean Atomic Number Background Estimates.

Scott Boroughs[1*]

[1.]Washington State University, School of the Environment, Pullman, WA, USA
*Corresponding author: scott.boroughs@wsu.edu

Phenocrysts can record the chemical evolution of their host magmas during their growth, and when carefully interrogated, provide insight into fractional crystallization, contamination, and recharge. The electron microprobe is an ideal tool for measuring chemical variation at the small scales necessary to resolve zoning in phenocrysts, but conventional methods of measurement (e.g. core–rim pairs, spaced transects, etc.) can provide an incomplete picture or be extremely labor and time consuming. Here, we present techniques for quantitatively mapping phenocrysts, for major, minor, and trace elements, which increase data density and continuity, without necessarily increasing analytical time.

Maps were acquired with ProbeImage [1] on the JEOL 8500F HyperProbe at WSU, using wavelength dispersive spectrometers. Maps were processed in CalcImage [1], which applies all matrix and interference corrections from a Probe For EPMA (PFE)[1] analysis setup to each pixel. Standards are acquired in PFE and mean atomic number (MAN) background estimates were used for background intensities. By measuring the peak intensity on a series of carefully selected standards, absent the analyte or its interferences, a background intensity vs MAN curve is established. PFE uses the established curve to determine the background intensity for each element [2], without the need to measure high/low off-peak backgrounds for interpolation to on-peak intensity, reducing count time by half.

Precision and detection limits (P/DL) are primarily a function of count rate, which in turn is a function of the elements of interest, spectrometer setup, dwell time, and beam current; though with some reconnaissance, P/DL can be estimated in advance and conditions tailored for a particular need. For reference, we performed mapping on BCR-2G [3] to assess P/DL over a wide range of elements and concentrations (Fig. 1).

Conventional spot analyses generally include significant time not spent counting the peak intensity (i.e. overhead), in the form of spectrometer movements, stage backlash, current measurements, et al. When mapping, there is essentially no overhead, as the instrument is set in a single configuration for the entire map, and any changes occur only once between passes. Overhead accounts for 40-95% of analysis time in conventional analyses, though MAN backgrounds are ~35-75% faster than off-peak backgrounds (Fig. 2). MAN backgrounds greatly reduce analysis time on unknowns, but they require additional standardization time up front, so they are most efficient for mapping and large data sets.

The first example of how quantitative mapping can interrogate magmatic processes is based on 1) sanidine from a Western Snake River Plain (WSRP) rhyolite lava, and 2) andesine from the Columbia River Basalt Group (CRBG). Barium in feldspar is an ideal candidate for quantitative mapping, as it is a relatively abundant trace/minor element, and it can be detected using two different diffracting crystals for maximum setup flexibility. We calculated anorthite (An), albite (Ab) and orthoclase (Or) content maps (Figs. 3, 7A), then used an empirically derived relationship between feldspar composition and Ba

https://doi.org/10.1017/S1431927622002707 Published online by Cambridge University Press

distribution coefficient (D-Ba) to calculate D-Ba for each pixel in the maps (Figs. 4, 7B), and in turn, Ba concentration in the host melts (Figs. 6, 8).

In the WSRP rhyolite, the major element chemistry of the feldspar is relatively consistent from the core to rim, with the exception of oligoclase inclusions in the center (Fig. 3), and consequently, D-Ba remains consistent (Fig. 4). The initial melt had a Ba concentration of ~400 ppm, which gradually increased to ~850 ppm, and then remained relatively steady (Fig. 6). The oscillatory zoning pattern may be the result of local depletion of the melt during crystal growth, and not necessarily changes in the bulk Ba concentration.

In the CRBG andesine, the Ba concentration in the liquid is relatively consistent (0.5-0.7 wt%) throughout crystal growth until the composition changes to sanidine at the rim, and D-Ba dramatically increases. Despite little change in melt Ba concentration, this results in ~4 wt% Ba in the feldspar rim, and subsequently an overall depletion of Ba in the melt (Fig. 8).

A second example of the utility of quantitative mapping involves a complex phase cluster found in a WSRP rhyolite lava. By combining various quantitative elemental maps in RGB color space (Fig. 10), phase distribution (Table 1) and composition (Table 2) can be quantified with high precision for applications including thermometry, barometry, and mass balance. With appropriate instrument setup, these tools can be applied at scales from sub-mm to full thin sections, and after maps are output, subsequent data reduction and analysis can be performed by the end user with easily accessible software (e.g Photoshop, Excel, ImageJ, et al.).

In conclusion, by utilizing mapping and MAN backgrounds, extremely dense data sets can be produced in a fraction of the time required by conventional spot analyses. Though visually striking, generating maps of entire crystals is not always necessary. Time can be exponentially reduced by mapping narrow, representative “strips” across phases with consistent zoning, allowing for higher P/DL or more spatial resolution. In relatively homogeneous matrices (e.g. quartz, olivine, garnet), one need not even measure every major element, and instead can specify some/all of their concentrations for matrix correction purposes. This frees up spectrometers to count for trace/minor elements, allowing better detection limits and precision. The ability of mapping to differentiate and quantify complex phase assemblages is also a powerful tool for petrologic modeling, allowing for precise modal analysis of even the smallest phases, which often exert disproportionate influence on the chemical evolution of magmas.

https://doi.org/10.1017/S1431927622002707 Published online by Cambridge University Press

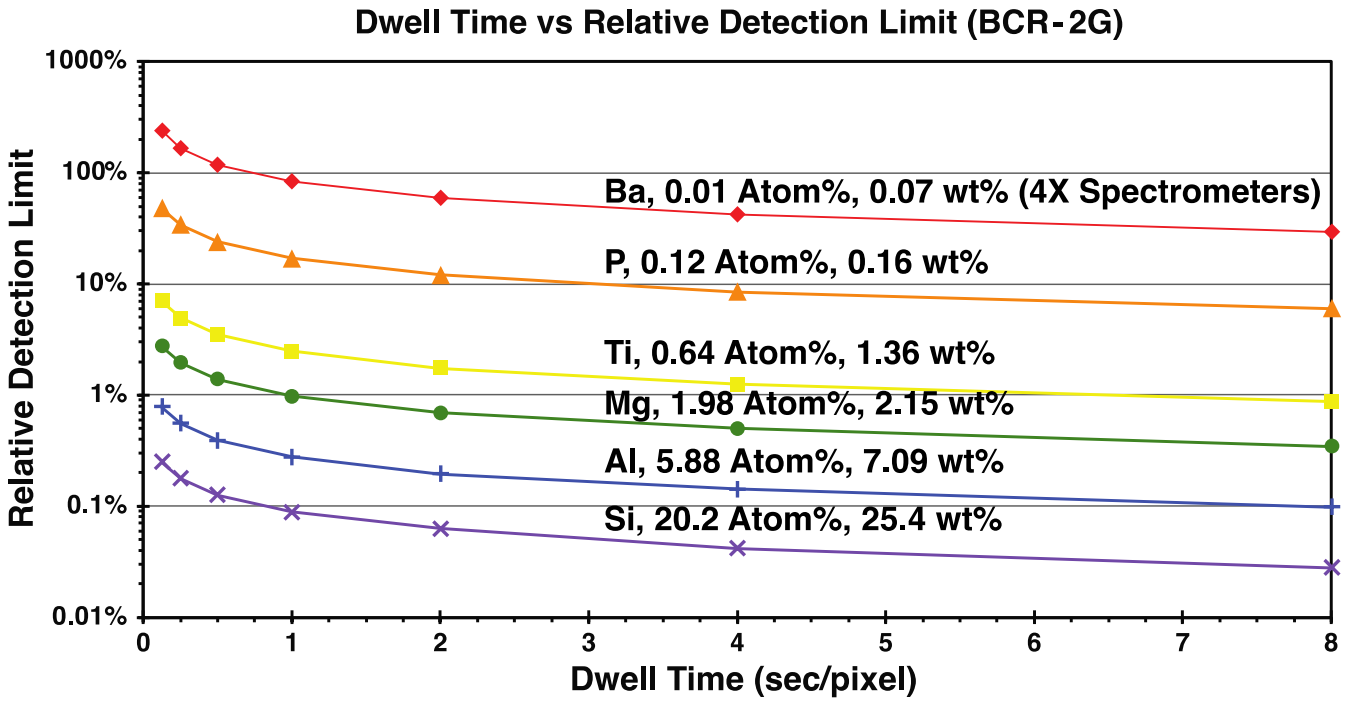

Figure 1. Dwell time vs relative detection limit (RDL). A series of maps with different dwell times were collected on BCR-2G, and RDL was calculated by dividing the detection limit by the concentration.

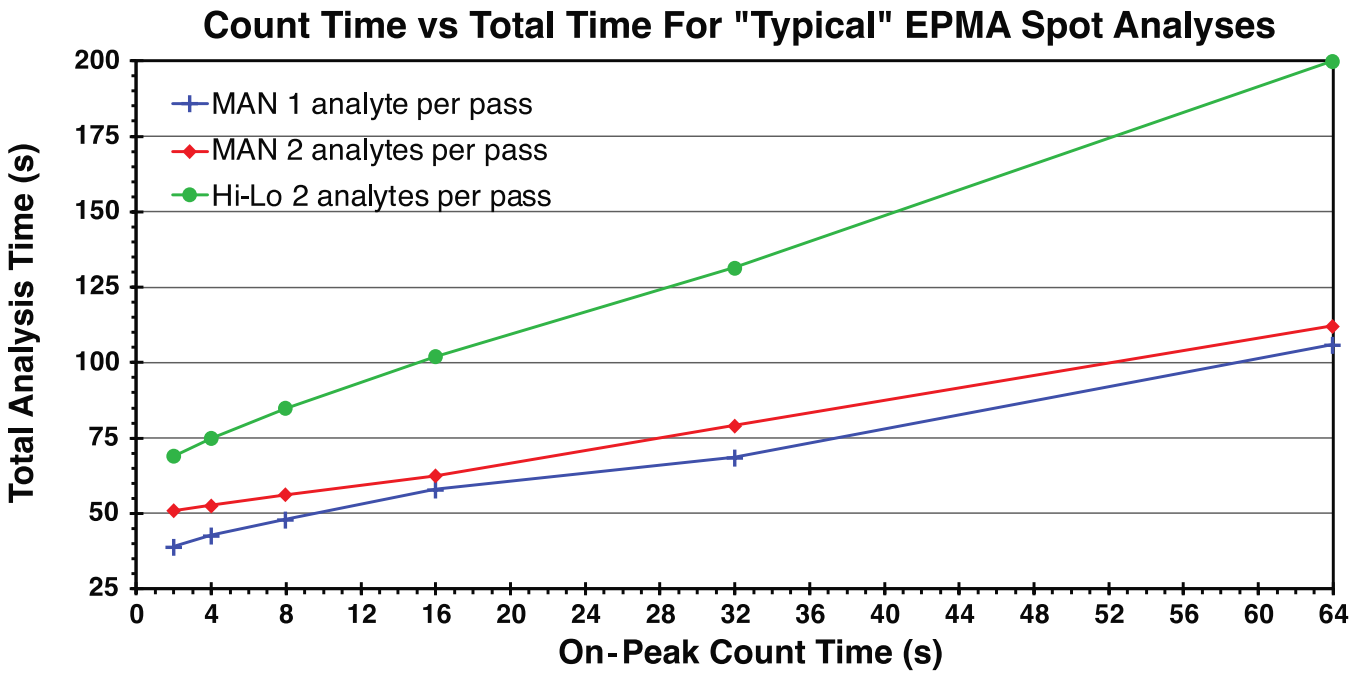

Figure 2. On peak count time vs total analysis time for spot analyses. Setups had 1-2 analytes per spectrometer, with nominal spectrometer travel distance ≤ 1/4 of total travel.

https://doi.org/10.1017/S1431927622002707 Published online by Cambridge University Press

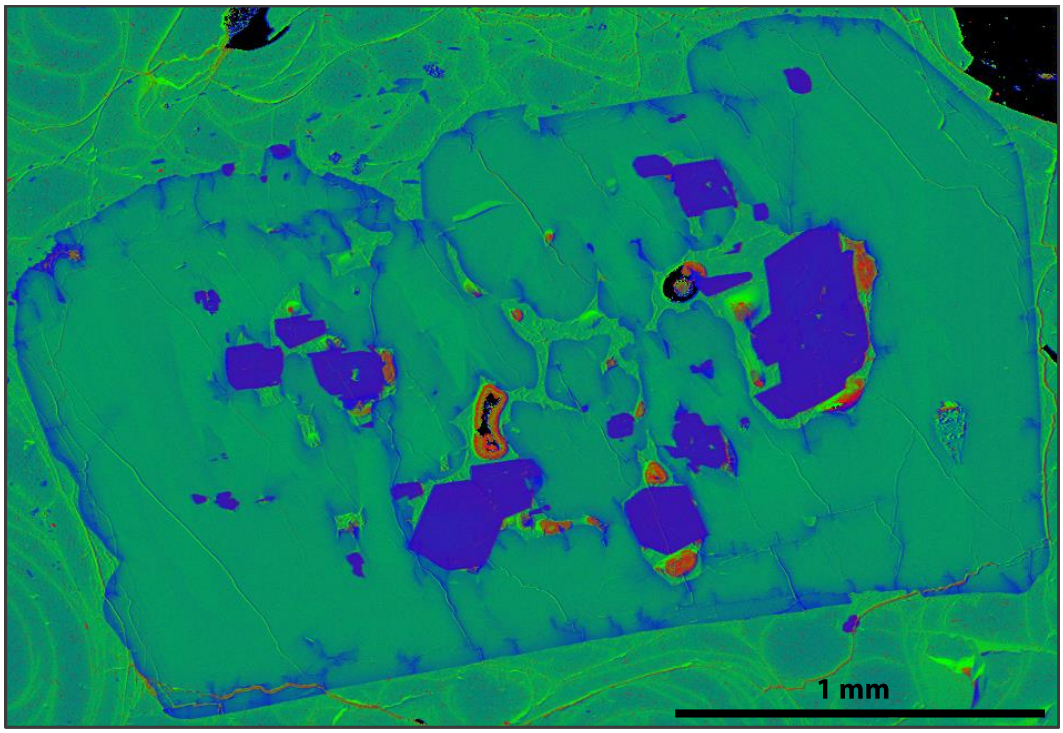

Figure 3. False color image of An-Ab-Or content in WSRP sanidine. Quantitative maps of Ca, Na, and K were used to calculate An, Ab, and Or, then each map was assigned as a channel in RGB color space. R = An, G = Or, B = Ab.

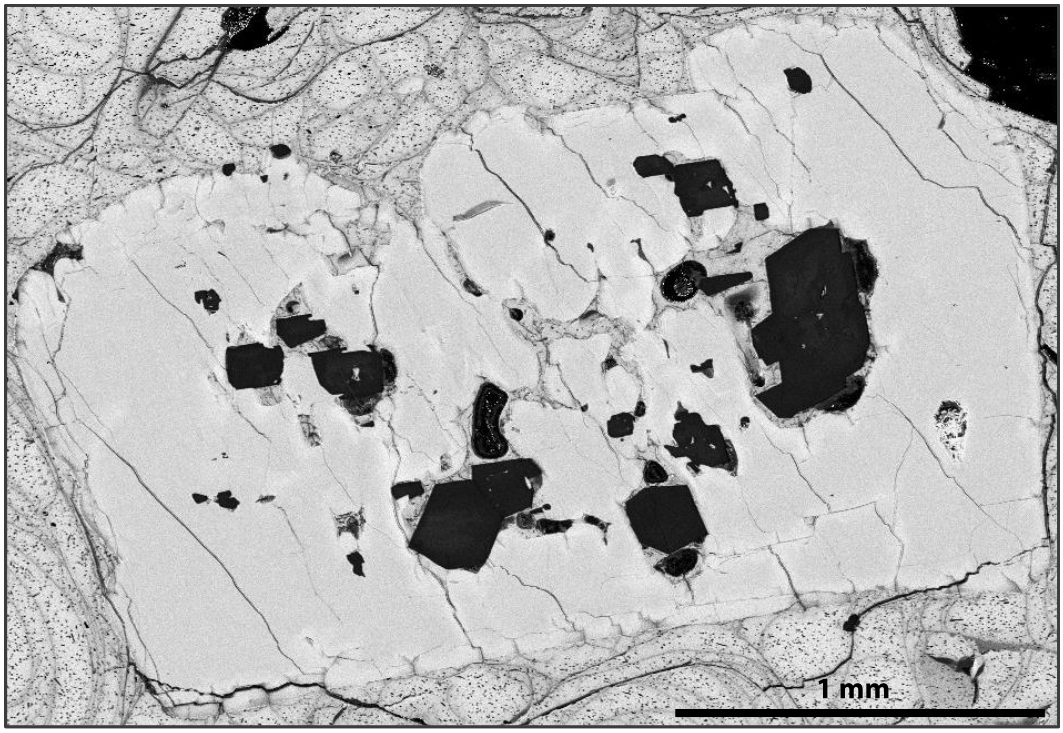

Figure 4. Map of Ba distribution coefficient (D-Ba) in WSRP sanidine. D-Ba was calculated for each pixel using quantitative map data for An and Or, and an empirically derived formula for the compositional dependence of D-Ba.

https://doi.org/10.1017/S1431927622002707 Published online by Cambridge University Press

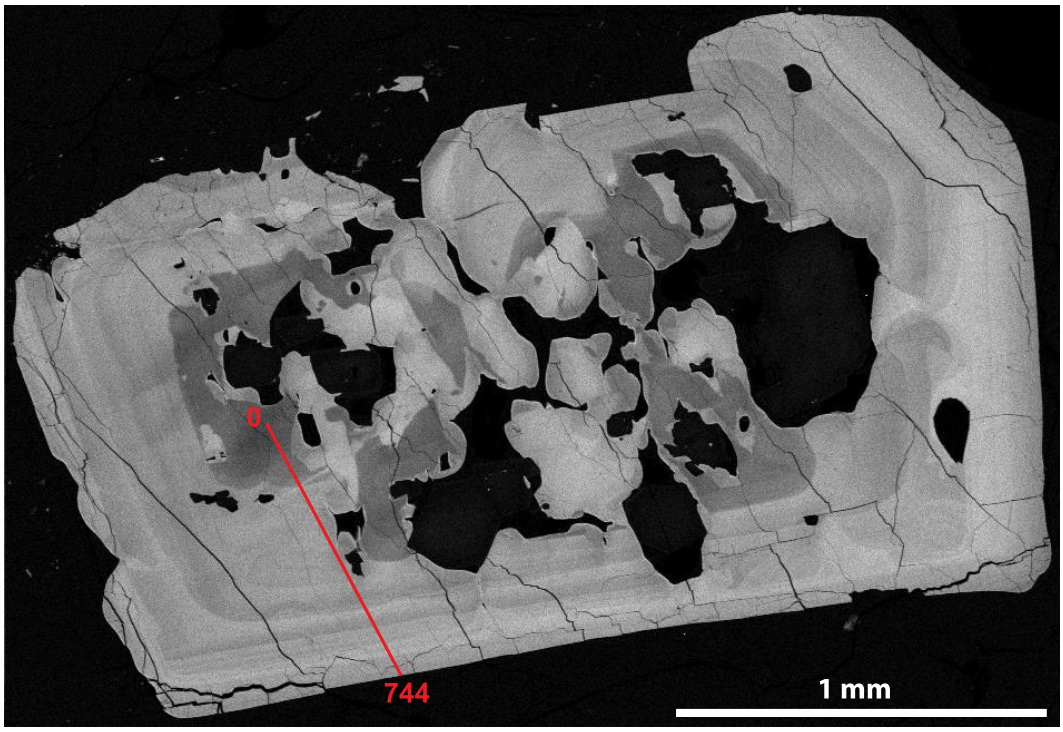

Figure 5. Map of Ba concentration in WSRP sanidine. 3 µm pixels. Acquired with Ba on four WDS spectrometers simultaneously. Dwell time 0.5 sec/pixel. Detection limit ~800 ppm. Red line represents profile from figure 6.

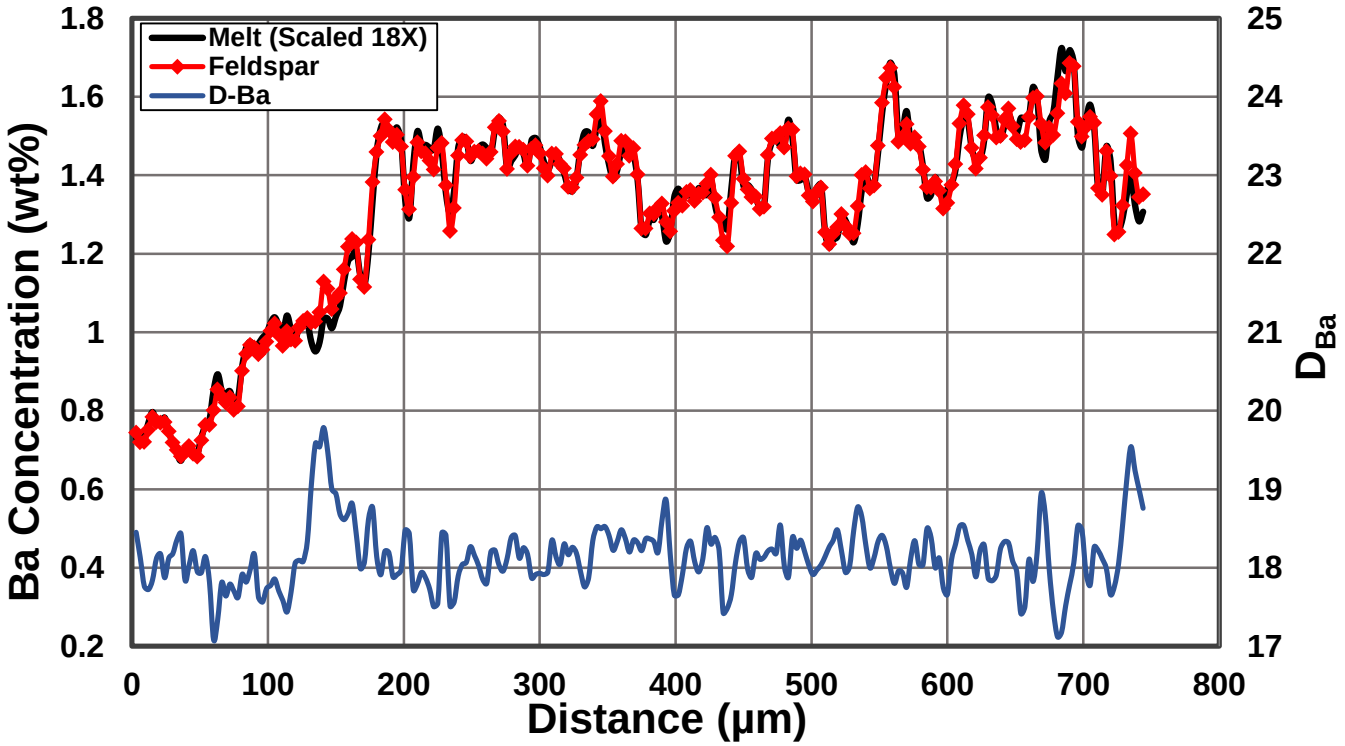

Figure 6. Profiles extracted from Ba concentration (Fig. 4) and D-Ba maps (Fig. 5) of WSRP sanidine. The calculated melt composition (black line) is scaled by the average D-Ba value (~18X) to plot at the same magnitude as the Ba concentration.

https://doi.org/10.1017/S1431927622002707 Published online by Cambridge University Press

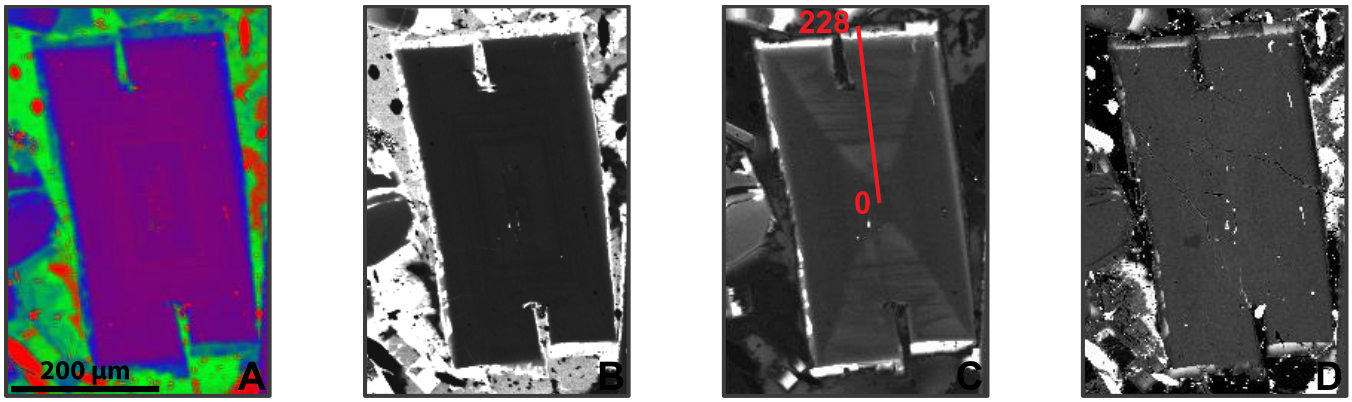

Figure 7. Maps of CRBG andesine. A) False color RGB image of An=R, Or=G, and Ab=B. B) Map of D-Ba. C) Map of Ba concentration. Red line represents profile from figure 8. D) BSE image. Note inadequate contrast to clearly see zonation visible in quantitative maps.

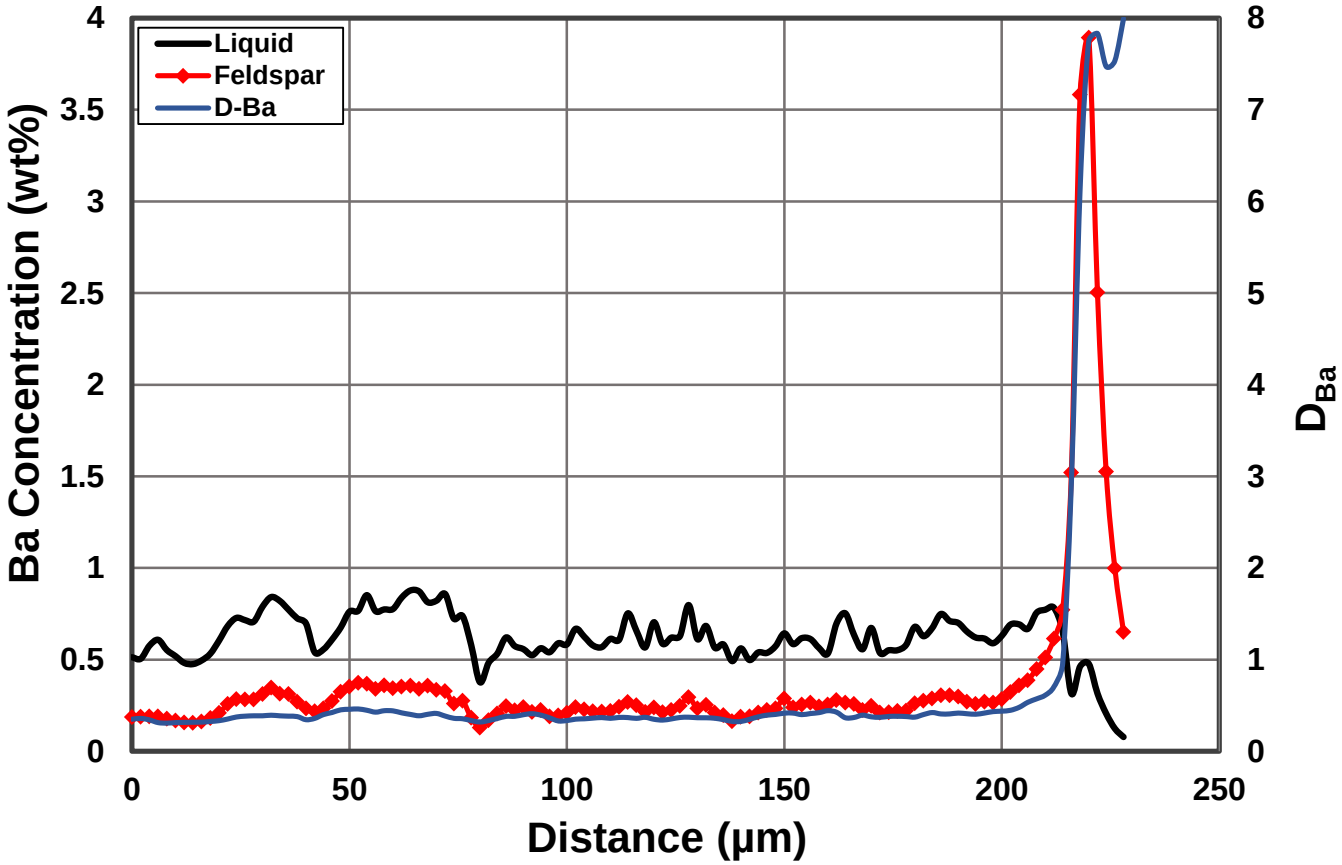

Figure 8. Profiles extracted from Ba concentration and D-Ba maps of CRBG andesine (Fig. 7B-7C).

https://doi.org/10.1017/S1431927622002707 Published online by Cambridge University Press

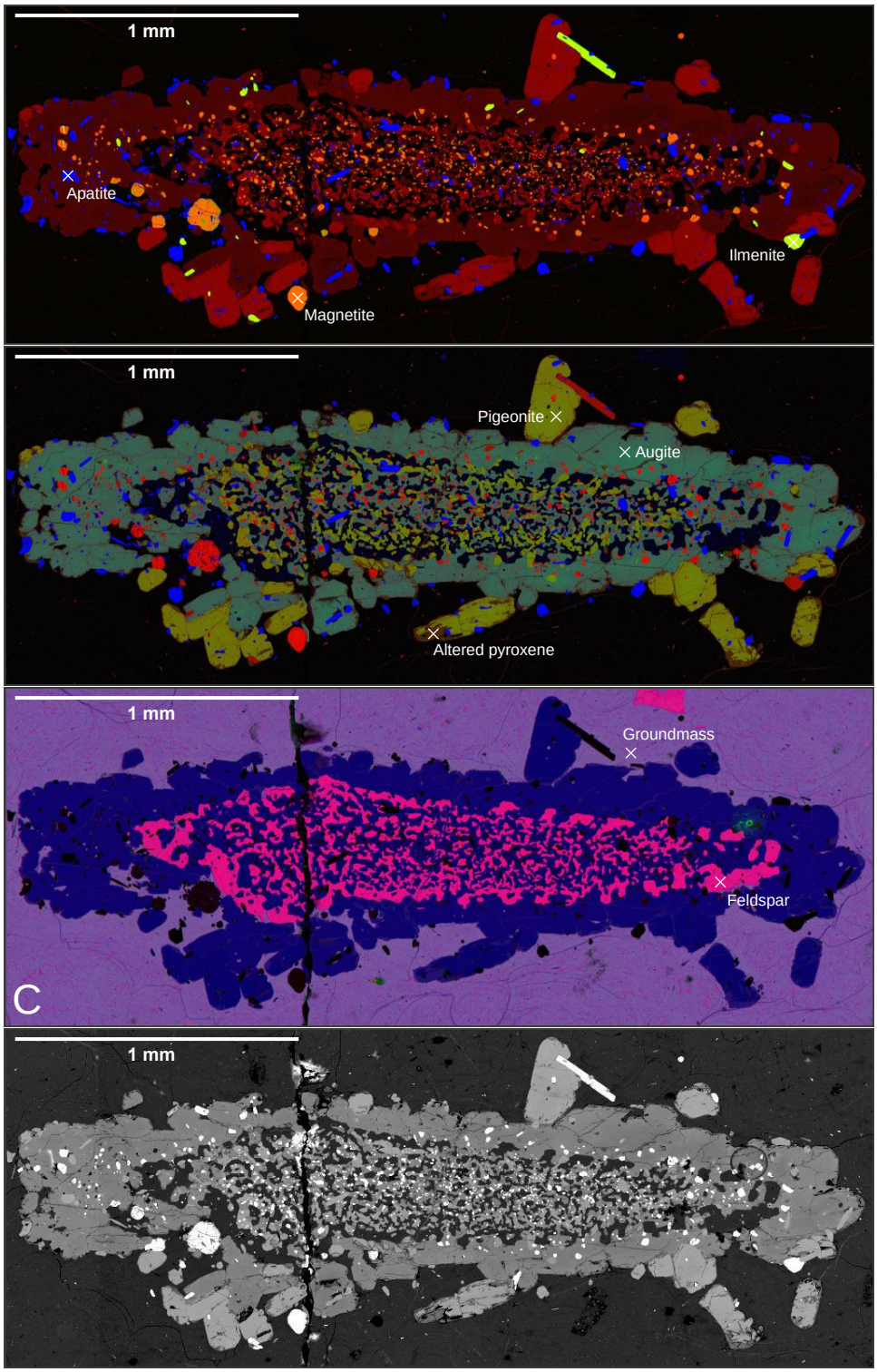

Figure. 9 False color and BSE images of a complex phase cluster from a Western Snake River Plain rhyolite lava flow. RGB Images were created in Adobe Photoshop by assigning an individual element to each channel of RGB color space. A) R = Fe, G = Ti, and B = P. B) R = Fe, G = Mg, and B = Ca. C) R = Al, B = K, and G = Si. See Table 1-2 for representative compositions and modal abundance of each phase. D) BSE image. Note inadequate contrast to fully differentiate phases with similar MAN (e.g. ilmenite/magnetite, apatite/pyroxene, glass/feldspar).

https://doi.org/10.1017/S1431927622002707 Published online by Cambridge University Press

	Glass	Augite	Feldspar	Pigeonite	Magnetite	Apatite	Ilmenite
SiO_2	75.3	51.6	61.2	50.9	0.94	0.51	*BDL*
TiO_2	0.15	0.18	*BDL*	*BDL*	16.4	0.10	49.0
Al_2O_3	11.9	1.06	24.1	0.45	1.39	*BDL*	0.17
FeO	2.11	15.2	0.45	33.0	70.9	0.62	48.6
MnO	0.09	0.61	*BDL*	1.45	0.72	0.16	0.89
MgO	0.11	11.4	*BDL*	12.6	0.77	*BDL*	1.17
CaO	0.53	19.5	6.10	1.39	*BDL*	52.4	*BDL*
Na_2O	2.53	0.57	7.16	*BDL*	*BDL*	0.27	*BDL*
K_2O	5.93	0.01	1.15	*BDL*	*BDL*	*BDL*	*BDL*
P_2O_5	*BDL*	*BDL*	*BDL*	*BDL*	*BDL*	40.2	*BDL*
Total	98.6	100.1	100.2	99.9	91.1	94.3	99.6

Table 1. Representative compositions for each identified phase in complex cluster (*BDL = below detection limit)*. Data was extracted by identifying a suitable pixel coordinate using ImageJ [4], then using simple Excel formulas to extract that coordinate's concentration data from each elements' map file. Each phase is identified on the individual images (Fig. 9), and extracted pixels are marked with a white X.

Image (RGB)	Phase	Area %	Normalized
Al-K-Si	Groundmass	50.7%	50.4%
Fe-Mg-Ca	High-Ca Pyx	24.7%	24.6%
Al-K-Si	Feldspar	8.8%	8.8%
Fe-Mg-Ca	Low-Ca Pyx	8.5%	8.5%
Fe-Mg-Ca	Pyx Alteration	3.0%	2.9%
Fe-Ti-P	Magnetite	2.9%	2.9%
Fe-Ti-P	Apatite	1.6%	1.6%
Fe-Ti-P	Ilmenite	0.4%	0.4%

Table 2. Modal abundance of each identified phase in complex cluster. Data was extracted from the various RGB false color images (Fig. 9) using the Image Analysis tools in Adobe Photoshop, which allow the user to assign a pixel scale, automatically select pixels of like color, and record proportions of those selections.

References:

[1] Probe Software - https://probesoftware.com/
[2] Donovan, J.J., and Tingle, T.N., Microscopy and Microanalysis **2** (1996), p. 1.
[3] Rocholl, Alexander, Major and Trace Element Composition and Homogeneity of Microbeam Reference Material: Basalt Glass USGS BCR- 2G. Geostandards Newsletter, **22** (2007), p. 33.
[4] Rasband, W.S., 1997-2020. ImageJ, U. S. National Institutes of Health, Bethesda, Maryland, USA, https://imagej.nih.gov/ij/

https://doi.org/10.1017/S1431927622002707 Published online by Cambridge University Press